ANALYTICAL SCIENCES NOVEMBER 2019, VOL. 35

Original Papers

Preparation of Molecularly Imprinted Magnetic Graphene Oxide-Gold Nanocomposite and Its Application to the Design of Electrochemical Sensor for Determination of Epinephrine

Leila MARDANI, Mohammad Taghi VARDINI,† Moosa ES'HAGHI, and Ebrahim GHORBANI-KALHOR

Department of Chemistry, Tabriz Branch, Islamic Azad University, Tabriz 5157944533, Iran

In this study, a new molecularly imprinted polymer (MIP) based nanocomposite was synthesized then used to determine epinephrine (EPN) by the use of an electrochemical sensor modified by it. Typical techniques for the synthesis of MIP have disadvantages, such as weak binding sites, low mass transfer and low selectivity. One of the ways to improve electrochemical properties is the use of graphene oxide (GR-Ox) and modification of its surface. For this purpose, GR-Ox was initially magnetized (MGR-Ox), then its surface was coated with a silica layer, and gold nanoparticles (AuNPs) were coated on its surface. Subsequently, copolymerization of methacrylic acid (MAA) and *N*,*N*′-methylene-bis-acrylamide (MBA) in the presence of EPN was performed on the MGO-AuNPs surface. Afterwards, a selective carbon paste electrode (CPE) with synthetic nanocomposite was fabricated to detect EPN. Under optimal conditions, a linear range from 10^{-8} to 5.0×10^{-7} M was obtained for the measurement of EPN in urine and blood with a detection limit of 5×10^{-9} M ($S/N = 3$).

Keywords Epinephrine, electrochemical sensor, gold nanoparticles, molecularly imprinted polymer, cyclic voltammetry

(Received March 28, 2019; Accepted June 19, 2019; Advance Publication Released Online by J-STAGE June 28, 2019)

Introduction

Epinephrine [1-(3,4-dihydroxyphenyl)-2-methylaminoethanol] is an important substance secreted from the upper adrenal gland (central portion) and is a hormone neurotransmitter, which belongs to the catecholamines.[1] EPN plays a vital role in the functioning of the central nervous system (CNS), the kidney system and the cardiovascular system, and is involved in such processes as increase in heart rate, contraction of blood vessels, stretching of airways and participates in the fight-or-flight response of the sympathetic nervous system.[2] A Low level of ENP is the cause of Parkinson's disease.[3] EPN regulates the immune system, heart rate, glycogen metabolism, lipolysis, and at most its level is indicative of specific diseases.[4,5] Therefore, research on this hormone is of importance in medical science and for human life.[6]

Various methods such as flow injection,[7,8] high performance liquid chromatography,[9,10] fluorimetry,[11] chemiluminescence,[12] spectrophotometry,[13,14] and capillary electrophoresis[15] have been used in pharmacological samples to determine EPN. However, the application of these methods is limited due to a complex matrix of samples, high prices and several obstacles to the implementation of the analysis. Meanwhile, electrochemical methods have been widely researched by researchers because of the sensitivity. GR-Ox has become one of the most attractive and popular materials in recent years due to its individual, physical and chemical properties, such as high surface area, ease of dispersion in organic solvents, water and different matrixes, appropriate electrocatalytic activity and high mechanical properties.[16] GR-Ox is widely used as a composite filler due to its unique features. It is clear that GR-Ox has very strong potential as a polymer filler to enhance mechanical, chemical and electrical properties.[17,18] The GR-Ox surface functionalization is typically performed to increase its capability of distribution.[19] However, composite-based GR-Ox has both advantages; a unique feature of GR-Ox and specific functional groups on its surface. In fact, it provides a new way to develop nanoscale electrochemical devices that have not been widely studied so far.[20,21] The electrochemical analysis is susceptible to electro-active molecules. Beyond sensitivity, it has the power to detect selectively different molecules that can be oxidized or reduced in various potentials.[22]

Recently, MIPs-based electrochemical sensors have attracted much attention because of their high selectivity, high sensitivity, small size and low prices.[23,24] Although MIPs prepared by the conventional method show high selectivity, they have some disadvantages, such as labor-intensive preparation process, complex preparation processes, low binding capacity, poorly available sites and slow kinetics.[25] Efforts to overcome these problems involvde the use of MIP-grafted GR-Ox sensors, which offer promising solutions for the research world of science.[26] For example, Mehdinia and colleagues have used GR-Ox as an electrochemically active substance and MIP as an element of identification in their sensor design.[27] In the last decade, metal nanoparticles have been used in the design of nanocomposites.[28,29] They have unique features including high adsorption capability, excellent electrical characteristics and small size.[30,31] Magnetic nanoparticles (MNPs) coated with

† To whom correspondence should be addressed.
E-mail: mtvardini@iaut.ac.ir

MIPs, and synthesized chemicals could be insulated by the use of an external magnetic field.[32] Therefore, a compound is quickly dissipated by magnetization, then the MIP provides a powerful analytical device with simplicity, flexibility and selectivity.[33]

In this work, a new material composed of MGR-Ox-AuNPs and MIPs was synthesized by employing EPN as a template molecule, then an electrochemical sensor was designed to measure EPN in biological samples. In the first step, GR-Ox was prepared from graphite. Then, MNPs were synthesized on its surface. Afterwards, MGR-Ox-SH was obtained by the coupling of thiosilica groups on the surface of nanoparticles by 3-mercaptopropyl trimethoxy silane (3-MPTS). In order to enhance the selectivity of MGR-Ox-SH, AuNPs were coated on the surface, such that they serve as backing materials in the high-performance synthesized polymer matrix of MGR-Ox-AuNPs@MIP. This nanocomposite is used to prepare CPE to measure EPN. This nanocomposite has been characterized by SEM and FT-IR. Cyclic voltammetry (CV), differential pulse voltammetry (DPV) and electrochemical impedance spectroscopy (EIS) were employed to study the electrochemical behavior of the fabricated sensor. The prepared sensor has shown high selectivity and sensitivity toward EPN. After optimization, the designed sensor exhibited a wide linear range and low detection limit and acceptable recovery for the EPN determination in real samples.

Experimental

Reagents and chemicals

Natural graphite powder, EPN and 3-mercaptopropyl trimethoxy silane (3-MPTS) were purchased from Sigma-Aldrich Co. (St. Louis, MO). Nitric acid (HNO_3), hydrochloric acid (HCl), sulfuric acid (H_2SO_4), hydrogen peroxide (H_2O_2), anhydrous ethanol, ferric chloride ($FeCl_3$), ferrous chloride ($FeCl_2$), chloroauric acid ($HAuCl_4$), trisodium citrate, toluene, ammonia, ammonium persulfate (APS), *N*,*N*′-methylene-bis-acrylamide (MBA), methacrylic acid (MAA), acetonitrile, potassium nitrate (KNO_3), ammonium chloride (NH_4Cl), lithium chloride (LiCl), potassium chloride (KCl), ammonium nitrate (NH_4NO_3) and paraffin were purchased from Merck. All solutions were prepared with ultrapure water.

Apparatus

The MGR-Ox-AuNPs@MIP nanocomposites were characterized by scanning electron microscopy (SEM, S-2500, Hitachi High-tech International Trading Co., Ltd., Shanghai, China). Electrochemical measurements were performed on the electrochemical workstation (PGSTAT302N, Netherlands). The FT-IR spectra were recorded by a Jasco FT-IR 6600 spectrometer. The electrochemical impedance spectroscopy (EIS) measurements were performed using a 0.02 M $[Fe(CN)_6^{-3/-4}]$ solution (frequency range: 0.1 to 10000 Hz, signal amplitude: 0.01 V). Electrochemical measurements were carried out based on a typical three-electrode system, using a modified CPE as working electrode, platinum electrode as an auxiliary electrode, and Ag/AgCl, KCl as a reference electrode.

GR-Ox, MGR-Ox synthesis

For the synthesis of GR-Ox, graphite was oxidized by the modified method of Hummer.[34] MGR-Ox was prepared according to the following procedure. Briefly, 350.0 mg $FeCl_2$ and 500.0 mg $FeCl_3$ were added to 100.0 mL deionized water in the presence of 50.0 mg GR-Ox under a nitrogen atmosphere. The mixture was heated up to 90°C, 20.0 mL 30% NH_3 was added to the mixture, then the suspension was stirred for 2 h. The pH of the mixture was controlled, the temperature was maintained below 90°C and the resulting mixture was stored under these conditions. The product was washed several times with 100.0 mL 0.1 M NaCl, then washed by ethanol and distilled water for 3 – 4 times. Eventually, the precipitate was dried under vacuum at 60°C.

Functionalization of MGR-Ox with a silica layer

In brief, 100.0 mg MGR-Ox was stirred in 50.0 mL toluene for 1 h, then 3.0 mL 3-MPTS was added. The solution was heated and subjected to reflux under a temperature of 85°C for 48 h and finally, to obtain silanized GR-Ox, the suspension was washed several times with toluene then, dried at 60°C.

Synthesis of MGR-Ox-AuNPs

AuNPs were synthesized with the reduction method using trisodium citrate, which has been previously reported. First, 4.0 mL 0.01 M $HAuCl_4$ solution was mixed with 150.0 mL deionized water and heated up to 100°C. Afterwards, 3.5 mL trisodium citrate (1 w/w %) was added and heated up to boiling point. When the color of the solution changed to red-wine, it was kept at the same temperature for 3 – 4 min, then the heat was removed and stirring continued until the solution had cooled. The average size of AuNPs was about 20 nm. MGR-Ox-AuNPs were obtained by mixing 100 mg of MGR-Ox with 15.0 mL of gold colloids while stirring for 2 h.

Synthesis of MGR-Ox-AuNPs@MIP

In this study, EPN, MAA, MBA and ammonium persulfate were applied as the template, functional monomers, cross-linkers and radical initiator in the polymerization process, respectively. At first, 100.0 mg MGR-Ox-AuNPs was added to 40.0 mL of deionized water, placed in an ultrasonic bath for 15 min then 0.2 mmol EPN was added and stirred intensively for 10 min. In the next step, 0.8 mmol functional monomer, 4.0 mmol cross-linker and 150.0 mg of the radical initiator were added to the reaction mixture, and it was refluxed at 60°C for 24 h. The synthesis steps of MGR-Ox-AuNPs@MIPs nanocomposite are shown in Scheme 1. The mixture was washed with 0.1 M HCl solution to remove the template molecule from the polymer network, and then dried at 60°C

In order to compare the MIP and non-imprinted polymer (NIP), MGR-Ox-AuNPs@NIP was synthesized using the same procedure with the only difference being not using the template molecule during the polymerization process.

Preparation of CPE from synthesized nanocomposite

The CPE was prepared by adding 100.0 mg graphite powder and 5.0 mg of MGR-Ox-AuNPs@MIP, which were mixed in a porcelain mortar for 10 min, then 95.0 mg of paraffin oil was added and stirred for 20 min for homogenization. This material was packed in a Teflon tube of 3 mm in diameter, while the copper wire was placed in the middle of this tube. The electrode was dried at room temperature for 48 h. It is necessary to be noted that the CPE should be floated inside the supporting electrolyte for 2 h before measuring to minimize the background signal so that it can be prepared for measurement with CV and DPV.

Electrochemical measurement

All electrochemical measurements were applied using a three-electrode electrochemical system including working, auxiliary and control electrodes at room temperature. Also, the working

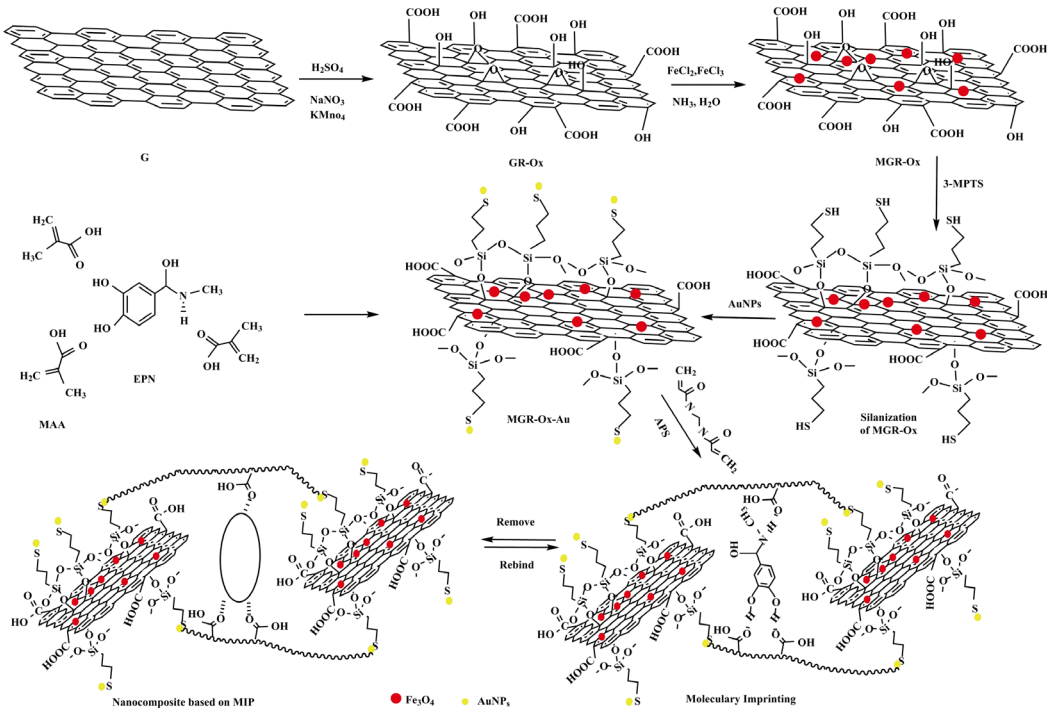

Scheme 1 Schematic representation for the preparation of MGR-Ox-AuNPs@MIP.

electrode was CPE fabricated from synthetic nanocomposite, the auxiliary electrode was platinum, and the control electrode was Ag/AgCl. Electrochemical techniques such as CV and DPV have been used to measure EPN with a modified CPE. EPN was dissolved in 0.1 M HCl, and 0.1 M KNO_3 were selected as the supporting electrolyte. CV and DPV were implemented with a potential scan of –2.0 to 2.0 V for detecting EPN.

The human serum and urine samples were prepared by using $ZnSO_4$–$Ba(OH)_2$ solution and acetonitrile solvent to eliminate the interfering proteins.[35,36]

Results and Discussion

Characterization of GR-Ox, MGR-OX, MGR-Ox-AuNPs, and MGR-Ox-AuNPs@MIPs

The details of the structure of the GR-Ox, MGR-Ox, MGR-Ox-SH, MGR-Ox-AuNPs and the MGR-Ox-AuNPs@MIPs nanocomposite are shown in Figs. 1 and 2 by FT-IR and SEM. The FT-IR spectrum of GR-Ox exhibits an absorption peak at 1197 cm^{-1}, which is related to the C–O bond, confirming the presence of the carboxylic group on the GR-Ox. The peaks at 1543 and 1692 cm^{-1} illustrate the C=C bond of unoxidized graphite remaining after the oxidation step. Sharp O–H peaks at 3742 cm^{-1} are due to the absorption of water molecules and hydroxyl groups of GR-Ox. The absorption peak at 1742 cm^{-1} is attributed to the C=O stretching bond (Fig. 1). SEM images of GR-Ox showed a sheet-like structure that leads to a high surface area (Fig. 2A). In Fig. 2B, the SEM image of prepared MGR-Ox is illustrated. As depicted in this image, the distribution of iron particles on the GR-Ox sheets is observable. The MGO surface morphology exhibited the aggregation of tiny grains, highly uniform in size and spherical shaped with a diameter of about 10 – 15 nm. In addition, FT-IR for MGR-Ox showed the presence of Fe_3O_4 in the structure of MGR-Ox based

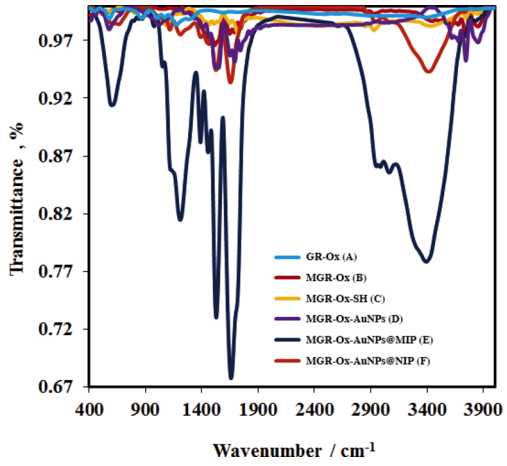

Fig. 1 The FT-IR spectra for GR-Ox (A), MGR-Ox (B), MGR-Ox-SH (C), MGR-Ox-AuNPs (D), MGR-Ox-AuNPs@MIP (E), MGR-Ox-AuNPs@NIP (F), respectively.

on the peak at 669 cm^{-1}, which is accompanied by vibration of the Fe–O bond (Fig. 1). The FT-IR spectrum of SH-functionalized MGR-Ox revealed a strong peak at 1086 cm^{-1}, which agreed with the asymmetric stretching vibrational of the Si–O–Si bond. It has shown peaks at 459 and 808 cm^{-1}, which are related to the symmetric stretching vibrational as well. Moreover, the S–H peak appeared at 2426 cm^{-1} (Fig. 1). Figure 2C indicates swollen MGR-Ox that correspond to the binding of (Fe_3O_4)–OH with 3-MPTS. Figure 2D shows Au NPs on the surface of the SH-functionalized MGR-Ox, while they are evenly distributed over the surface. Au NPs appear in spherical shapes with a size of 15 – 40 nm.

Furthermore, FT-IR spectrum of MGR-Ox-SH-AuNPs exhibited absorption peaks at 578 and 1017 cm^{-1}, which revealed

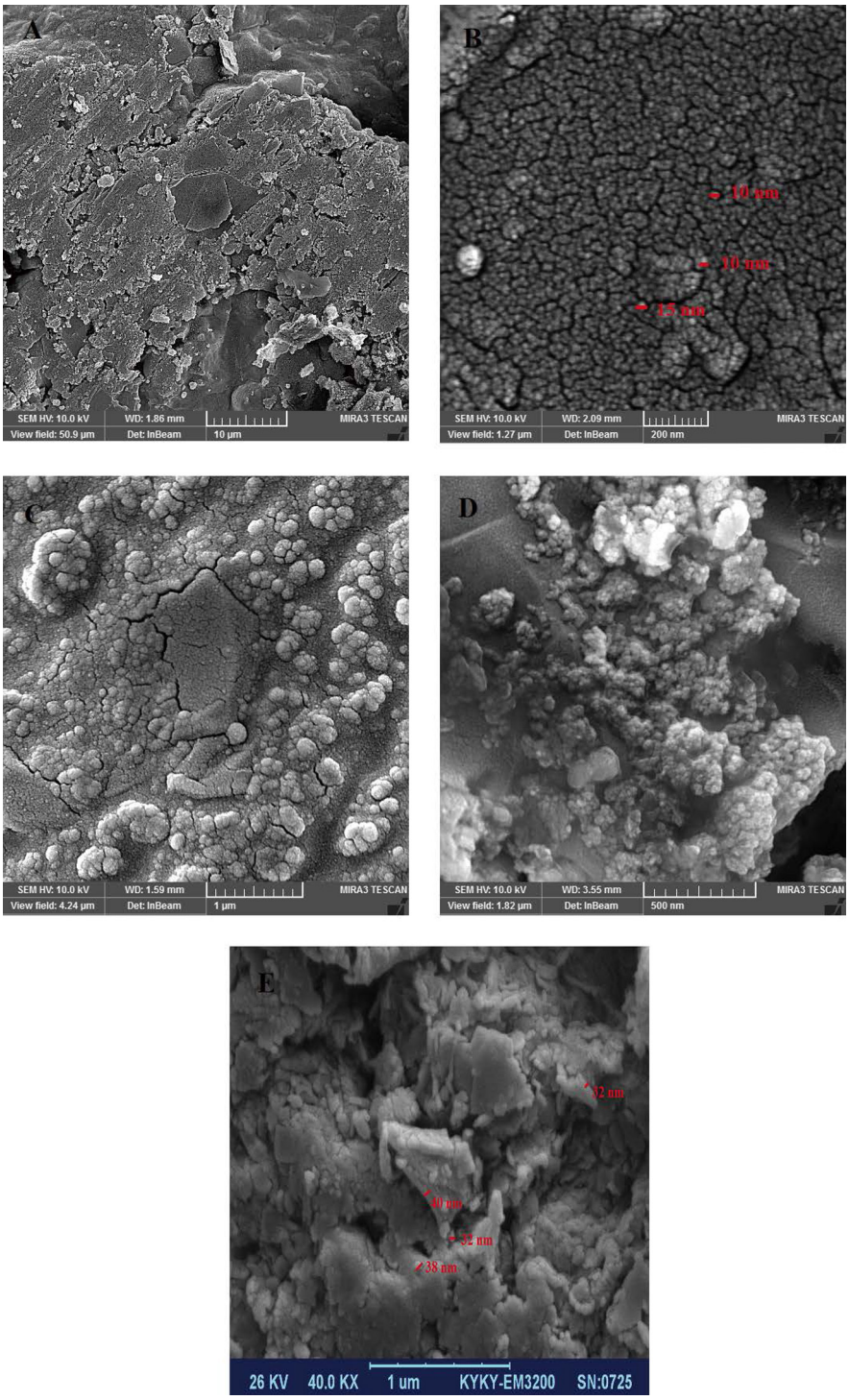

Fig. 2 SEM images of (A) GR-Ox, (B) MGR-Ox, (C) MGR-Ox-SH, (D) MGR-Ox-AuNP$_S$ and (E) MGR-Ox-AuNP$_S$@MIP.

the interaction between Au–S and Si–O–Au (Fig. 1). In Fig. 2E, SEM micrograph of MGR-Ox-AuNPs@MIP is depicted, which displays a thin film about 30 – 45 nm related to the MIP layer and confirms the successful synthesis of the nanocomposite. In the FT-IR spectrum of MGR-Ox-AuNPs@MIP, the peaks at 1117 and 1210 cm^{-1} indicate C–O–C and C–O bonds, respectively. A peak at 3392 cm^{-1} is related to phenolic O–H. The peak with a wave number associated with symmetric and asymmetric vibrations of C–H is 2984 cm^{-1}. The most critical point in the spectrum is at the wave number of 1659 cm^{-1}, which covers all the previous peaks and is related to the carbonyl of the polymer network (Fig. 1). There is a weak peak attributed to –OH in MGR-Ox-AuNPs@NIPs nanocomposite caused by the template molecule absence, but the peaks of other polymer components are present with slight movement in wavenumber according to the figure (Fig. 1).

Electrochemical characterization of electrodes

The electrochemical behavior of various modified electrodes was examined by CV in 0.02 M [$Fe(CN)_6^{-3/-4}$] solution.

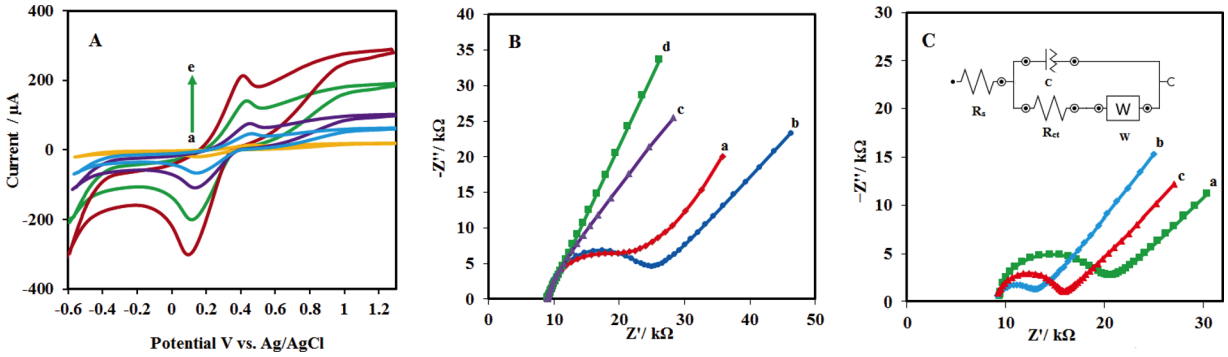

Fig. 3 (A) Cyclic voltammetry in 0.02 M $[Fe(CN)_6^{-3/-4}]$ solution: (a) pure graphite electrode, (b) GR-Ox, (c) MGR-Ox (d) MGR-Ox-Au and (e) MGR-Ox-Au@MIP electrodes. (B) Impedance spectra in 0.02 M $[Fe(CN)_6^{-3/-4}]$solution: (a) GR-Ox, (b) pure graphite, (c) MGR-Ox, and (d) MGR-Ox-AuNPs. (C) (a) MGR-Ox-AuNPs@MIP before removing EPN, (b) MGR-Ox-AuNPs@MIP after removing EPN and (c) NIP (pH 7.0, scan rate 0.1 V/s).

The scan rate was 0.1 V/s from –2.0 to 2.0 V. The CVs of different electrodes are displayed in Fig. 3A. The small peaks were illustrated at about 0.1 and 0.4 V (curve a). The GR-Ox electrode shows an increasing peak due to the lone electron pair of functional groups and the role of the semiconductor (curve b).[37] A significant signal from the MGR-Ox has been recorded, which shows that the conductivity of the electrode has increased with the addition of nanoparticles on the GR-Ox surface (curve c). When the AuNPs are coated on the MGR-Ox surface, the cathodic peak current is increased (curve d). The values of peaks potential gradually decreased because the MGR-Ox-Au electrode demonstrated excellent electron transport.[38] The efficacy of the AuNPs on the electrode surface is related to the intense electrocatalytic activity. In other words, the results confirmed that signals of electrodes increased with increasing metal nanoparticles and conductive materials.

We have applied the Randles–Sevcik equation for studying the electrochemically active surface area of the pure graphite electrode and modified electrodes in 0.02 M $[Fe(CN)_6^{-3/-4}]$ by cyclic voltammetry:[39]

$$I_p = (2.69 \times 10^5) n^{3/2} A D^{1/2} C v^{1/2} \quad (1)$$

Where (n) is the electron transfer number, (A) the surface area of the electrode, (D) the diffusion coefficient, (I_p) the peaks current, (v) the scan rate, and (C) is the concentration of $[Fe(CN)_6^{-3/-4}]$. Therefore, the active surface area was calculated as: 0.0706, 0.16, 0.41, 0.64, 0.74 cm^2 for pure graphite electrode, GR-Ox, MGR-Ox, MGR-Ox-AuNPs, and MGR-Ox-Au@MIP, respectively. The results proved that electrodes based on MGR-Ox-Au@MIP have high efficiency due to the provision of large active surface area.

Also, the EIS provides detailed information on electrodes' impedance variations to characterize the properties of the modified sensor.[40] In order to investigate the electron transfer capabilities of the pure graphite, GR-Ox, MGR-Ox and MGR-Ox-Au were used as electrode materials. Figure 3B illustrates the impedance spectra at different steps of sensor modification in the presence of 0.02 M $[Fe(CN)_6^{-3/-4}]$ solution. All Nyquist plots showed a distorted semicircle part at higher frequencies that indicated the charge-transfer resistance (R_{ct}) and followed by a linear portion at lower frequencies that shows the diffusion process.[41] The fitted value of R_{ct} obtained for pure graphite, GR-Ox, MGR-Ox and MGR-Ox-Au was 11.3, 14.2, 2.1 and 530.0 kΩ, respectively. The R_{ct} of the GR-Ox electrode is more extensive than pure graphite (Fig. 3B (a – b)), due to the disturbance of the electron transfer in sp^2 network.[42] Linear part at lower frequencies proved the presence of MGR-Ox, and AuNPs attributed to high diffusion of ferricyanide toward the electrode surface (Fig. 3B (c – d)). The sharp slopes show that ionic conducting solution have improved.[43] EIS results are in good agreement with CVs in $[Fe(CN)_6^{-3/-4}]$ (Fig. 3A). Based on the results, MGR-Ox-Au was selected for synthesis of MIP.

The EIS results of MGR-Ox-Au@MIP and NIP electrodes are given in Fig. 3C. The fitted value of R_{ct} obtained for MGR-Ox-Au@MIP (before and after removing the template), and NIP was 8.5, 3. and 6.36 kΩ, respectively. The increasing value of R_{ct} indicates that MIP was synthesized on its surface (Fig. 3C (a)). In fact, MIP acts as an obstacle for the transfer of electrons between electrode and electrolyte. After removing the template, R_{ct} has decreased due to the formation of cavities and the ease of transmission of electrons (Fig. 3C (b)). Moreover, the synthesis of NIP on the surface of MGR-Ox-Au shows R_{ct} is between MIP (before removing template) and MIP (after removing template) (Fig. 3C (c)). The phenomena confirmed that the surface of the electrode prevented the transfer of electrons. In other side formation NIP without template might improve the transfer of electrons.[44] Also, slopes of e–g are enhanced owing to improved ionic diffusion.

Optimization of the preparation of electrochemical sensors and measurement conditions

Optimization of the amount of MGR-Ox-AuNPs@MIPs in the sensor. There is a relationship between the peak currents of EPN and the amount of MGR-Ox-AuNPs@MIP on the CPE, as peak current increases by decreasing the nanocomposite. The highest current was recorded in different solutions of EPN when the nanocomposite amount diminished to 5.0 mg (Figs. 4A – 4C). However, when the amount of nanocomposite in the sensor was more than 40.0 mg, the current decreased dramatically because of the decrease in conductivity on the electrode surface. Also, the reason for this was the hydrophilicity of synthetic polymer. When the amount of nanocomposite increased, the surface of the electrode was inflated, and the available binding sites were destroyed. As a result, 5.0 mg of nanocomposite was used for the carbon paste electrode.

Effect of molar ratio of template molecule to functional monomer. The molar ratio of template molecule to the functional monomer

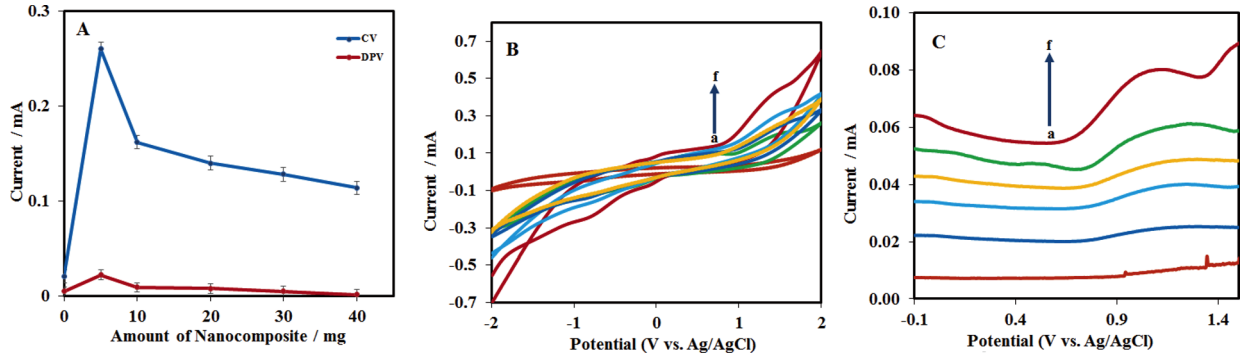

Fig. 4 (A) Effect of the amount of nanocomposite on the modified electrode. (B) and (C) CVs and DPVs of the modified electrode with different amounts of nanocomposite, respectively (a, 0 mg; b, 40 mg; c, 30 mg; d, 20 mg; e, 10 mg; f, 5 mg; pH 7.0; scan rate, 0.1 V/s).

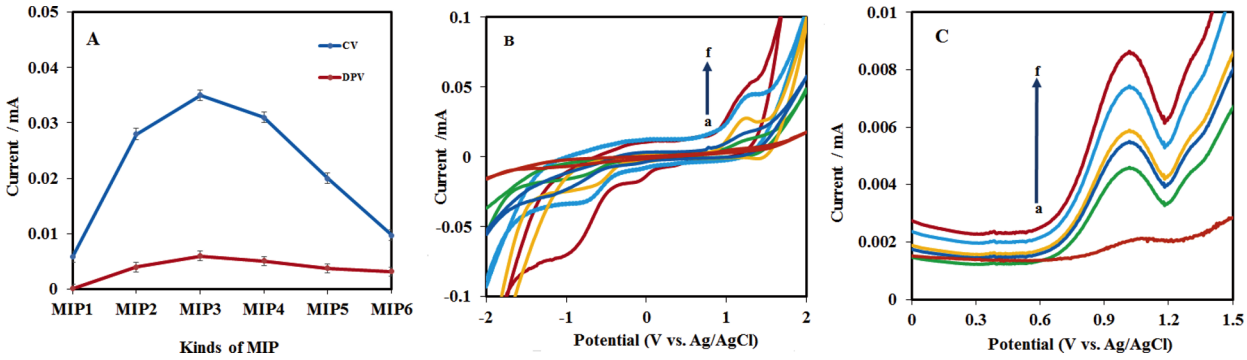

Fig. 5 (A) Effect of the molar ratio of template molecule to functional monomer on the modified electrode signal. (B) and (C) CVs and DPVs of the modified electrode with different molar ratios of template molecule to functional monomer, respectively (a, MIP_1 (1:2:20); b, MIP_2 (1:3:20); c, MIP_3 (1:4:20); d, MIP_4 (1:5:20); e, MIP_5 (1:6:20); f, MIP_6 (1:8:20); pH 7.0; scan rate, 0.1 V/s).

is important in the polymerization which controls the creation of sites. Different types of MIPs in different molar ratios have been prepared (MIP_1 (1:2), MIP_2 (1:3), MIP_3 (1:4), MIP_4 (1:5), MIP_5 (1:6), MIP_6 (1:8)). The EPN molecule contains three hydroxyl groups and one amino group, which can form hydrogen bonds with functional groups such as amino and carbonyl groups. The molar ratio of template to monomer should be higher than 1:3. At low molar ratio, it is difficult to create stable binding sites. Also, results showed that increasing the amount of monomer during polymerization improved the peak currents. This, in turn, causes proper binding sites to form in the polymer matrix. But peak current decreased in MIP_4, MIP_5 and MIP_6. This is similar to the fact that the number of interactions of the monomer with EPN increased during polymerization, which prevented the formation of sufficient cavities in the polymer. Therefore, the MIP_3 was used as the optimum MIP in all determinations (Figs. 5A - 5C).

Effect of pH on the peak current. An important factor in obtaining an electrochemical signal is pH. The effect of pH was investigated through the electrochemical signal of EPN in the modified electrode. EPN was measured at different pH ranges from 2.0 to 8.0 (Figs. 6A - 6C). The results confirmed the maximum current response at pH 7.0. The structure of the EPN was decomposed at levels higher than pH 7.0, and the current response decreased dramatically. At lower pH, the nanocomposite has a negative charge, and EPN is protonated. On the other hand, decreasing current at pH values less than 7.0 resulted in increasing electrostatic interactions between protonated template and MIP, compared with interactions between the template and MIP cavities. Consequently, EPN decreases on the surface of the sensor and the signal drops out. As a result, the best interaction between EPN and MIP cavity is at pH 7.0, which was considered as optimal in measuring EPN during the experiments.

Also, the cyclic voltammograms of EPN observed a relationship between current and potential at different pH as well as. With the increase in pH, peak potential shifted to negative values. A dependence of E_p on pH obeyed the following equations: $E_a = -0.0539\text{pH} + 1.5261$ ($R^2 = 0.9257$), $E_c = -0.0539\text{pH} - 0.05075$ ($R^2 = 0.9094$) (Fig. S1, Supporting Information). The slope of curves is found to be –0.0539 and –0.0539 for anodic and cathodic respectively, which is close to the theatrical value of 0.059 V/pH[45] and confirms that the number of electrons transferred and protons are equal.

Effect of scan rate on peak current. The influence of scan rate on the electrochemical behaviors of EPN was studied by CV at various sweep rates in pH 7.0 from –2.0 to 2.0 V. The anodic and cathodic peaks current of EPN increased with increasing scan rate (0.025 - 0.1 V/s) on modified electrode and showed a linear relationship with the $v^{1/2}$ with linear regression equation $I_a = (3.0 \times 10^{-4})v^{1/2} - 4.0 \times 10^{-5}$ ($R^2 = 0.9882$), $I_c = (-2.0 \times 10^{-4})v^{1/2} + 3.0 \times 10^{-5}$ ($R^2 = 0.9433$) for anodic and cathodic, respectively

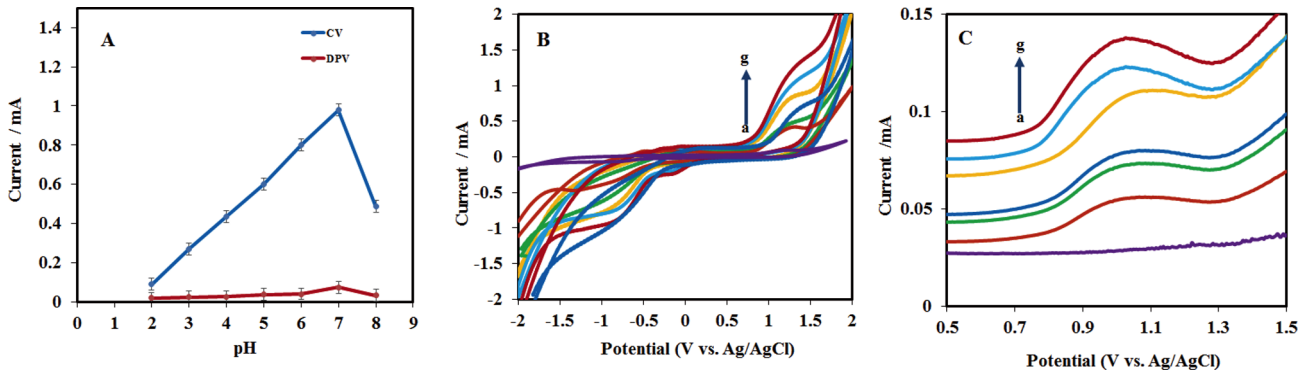

Fig. 6 (A) Effect of pH on the modified electrode signal. (B) and (C) CVs and DPVs, respectively of the modified electrode in different pH EPN solution (a, 2.0; b, 3.0; c, 4.0; d, 8.0; e, 5.0; f, 6.0; g, 7.0; scan rate, 0.1 V/s).

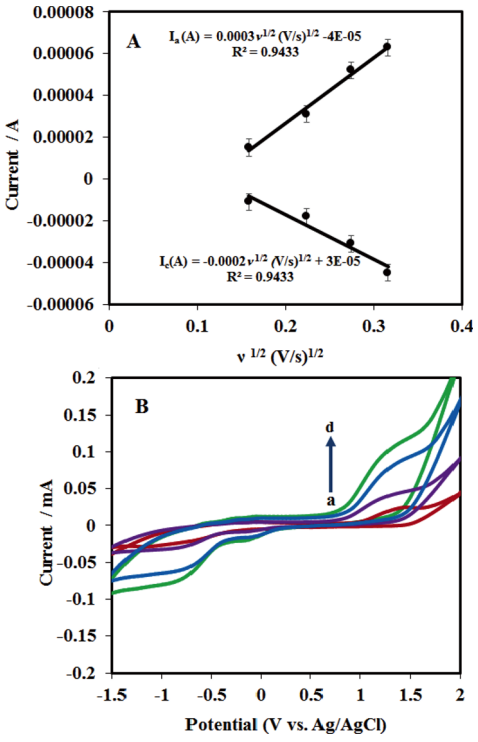

Fig. 7 (A) The plots of I_a, I_c *vs.* $v^{1/2}$ for the oxidition and reduction of EPN at surface electrode. (B) Cyclic voltammograms of 10^{-6} M EPN at modified electrode in KNO_3 (0.1 M) at different scan rates of (a) 0.025, (b) 0.05, (c) 0.075 and (d) 0.1 V/s, pH 7.0.

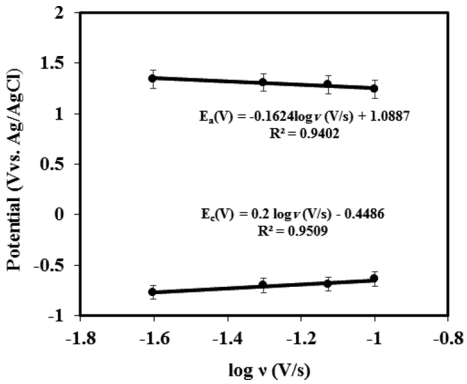

Fig. 8 Plot of E_p *vs.* logarithm of scan rate.

(Figs. 7A and 7B). The result indicates that the electron transfer reaction is controlled by the typical diffusion.[46] From the slope of the plot I *vs.* $v^{1/2}$ and using Eq. (1), value of the D for EPN was calculated as 2.16×10^{-6} cm^2/s.

According to the Laviron graph,[47] we can obtain information about the rate of electrochemical reaction [$E_a = -0.1624 \log v + 1.0887$, $R^2 = 0.9402$; $E_c = 0.2 \log v + 0.4486$, $R^2 = 0.9509$]. It is clear that with a decreasing scan rate, the anodic peak potential shifts to positive potential whereas the cathodic peak potential shifts negatively (Fig. 8). The curve of E_p *vs.* log v exhibites two straight lines with slopes of $2.3RT/(1-\alpha)nF$ and $-2.3RT/\alpha nF$, respectively, for anode and cathode. The value of the transfer coefficient (α) can be determined with regard to slopes of E_p *vs.* log v[48]:

$$\log \kappa_a/\kappa_c = \log \alpha/(1-\alpha) \quad (2)$$

Where κ_a and κ_c is the slope of straight lines for E_a *vs.* log v and E_c *vs.* log v, respectively. We obtained the transfer coefficient (α) 0.53 for the irreversible electrode process. Therefore, we found $n = 2$. Two electrons were affected in the electrochemical reactions. We can suggest a probable electrochemical mechanism of EPN (Scheme 2).[49,50]

In addition, the apparent heterogeneous electron transfer rate constant (k_s) can be determined by Eq. (2):[51]

$$k_s = \alpha nFv/RT \quad (3)$$

Considering the scan rate, transfer coefficient and number of electrons, the k_s value is obtained as 1.79 s^{-1} for EPN.

Optimization of the type and concentration of supporting electrolyte

Supporting electrolyte concentration is another important factor in the electrochemical analysis. In this study, CV was performed at 10^{-5} M EPN solution with different types of supporting electrolytes such as KNO_3, NH_4Cl, LiCl, NH_4NO_3, KCl at potential range of –2.0 to 2.0 V. According to observations, when LiCl was used, the color of the analysis solution changed and this is probably due to the interaction of NH_2 in EPN with Cl. When NH_4Cl and NH_4NO_3 were used as

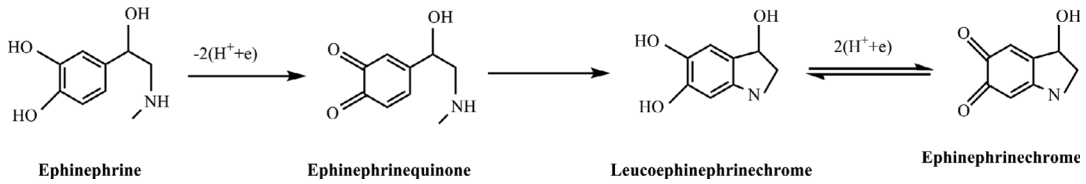

Scheme 2 The electrochemical mechanism of EPN at modified electrode with MGR-Ox-AuNPs@MIP.

Table 1 Analytical properties of different detection methods for determination of EPN

Method	Detection limit/M	Linear range/ M	Ref.
CV by glassy electrode modified	7.6×10^{-7}	10^{-5} – 50×10^{-5}	52
CV by gold electrode modified	5.1×10^{-7}	7.0×10^{-7} – 5.0×10^{-4}	53
Flow injection spectrophotometric	4.8×10^{-7}	6.4×10^{-6} – 3.0×10^{-4}	54
MGR-Ox-Au@MIP/CPE	5×10^{-9}	10^{-8} – 5×10^{-7}	This paper

supporting electrolyte, a buffering system was formed inside the solution, and it was complicated to change the pH of the solution. As a result, the KNO_3 concentration was investigated from 0.05 to 0.2 M. Also, the current is improved by increasing electrolyte concentration, but at 0.2 M, a color change occurred in the analyte solution. It is also likely that binding sites of MIP was saturated by charge carriers. Therefore, the interaction between nanocomposite and EPN was decreased by enhancing the concentration of the supporting electrolyte. In this regard, 0.1 M KNO_3 was selected as the optimum concentration of supporting electrolyte in subsequent experiments (Fig. S2, Supporting Information).

Calibration curve

In this study, DPV was selected for the calibration curve of EPN, because of higher sensitivity and lower limit detection than CV. Under the optimal conditions of the MGR-Ox-AuNPs@MIP sensor, a linear relationship between the current and the concentration of EPN in the range of 10^{-8} to 5×10^{-7} M was achieved with a correlation coefficient of 0.9897. It was wider and lower than the usual methods, as indicated in Table 1. The regression equation ($I = 139.44C + 0.0003$) was used to calculate the detection limit of 2.36×10^{-8} M from the signal-to-noise ratio of 3σ (since σ is standard deviation and $n = 3$) (Figs. 9A and 9B)).

Selectivity of the sensor

The effect of coexisting interferents was studied by testing the detection of 6×10^{-8} M EPN in solutions containing different concentrations of interference by the DPV method under the same experimental conditions. The results showed that 30-fold concentrations of uric acid (UA) and ascorbic acid (AA) produced no change on the signal of EPN. Since the structures of AA and UA have a clear difference compared with DA, the sites in the polymer could not bind them completely, which resulted in a much lower signal. Moreover, some 100-fold concentrations of ions such as Na^+, Mg^{2+}, Al^{3+}, NO^{3-}, SO_4^{2-} had no influence on the current of EPN. None of the structural

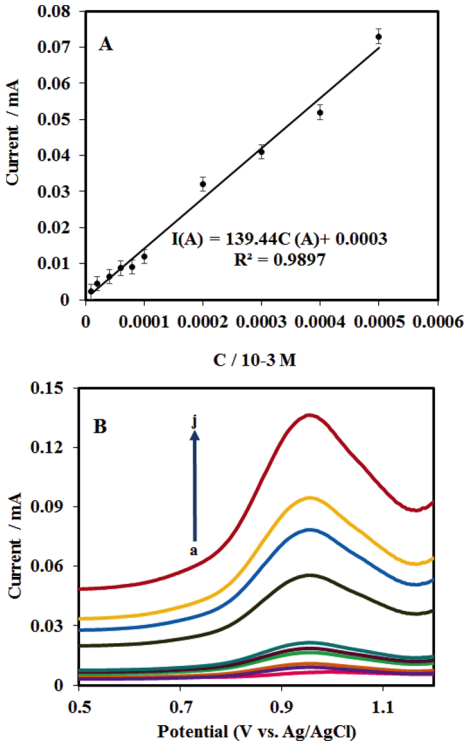

Fig. 9 (A) The linear relationship between the electrochemical signal and the concentration of EPN (the concentrations of EPN were: 10^{-8}, 2×10^{-8}, 4×10^{-8}, 6×10^{-8}, 8×10^{-8}, 10^{-7}, 2×10^{-7}, 3×10^{-7}, 4×10^{-7}, and 5×10^{-7} M, respectively). (B) DPVs in: 10^{-8}, 2×10^{-8}, 4×10^{-8}, 6×10^{-8}, 8×10^{-8}, 10^{-7}, 2×10^{-7}, 3×10^{-7}, 4×10^{-7}, and 5×10^{-7} M EPN solution (pH 7.0, scan rate 0.1 V/s).

analogs matched with the imprinted sites due to poor coordination of cavities in terms of the size and shape. Furthermore, to investigate the selectivity of the molecularly imprinted sensor, we found some of the similar substances with EPN in the biological fluids, such as isoproterenol (IP), dopamine (DA) and noradrenalin (NE). Figure S3 (Supporting Information) illustrates the selectivity of the MGR-Ox-Au@MIP and MGROx-Au@NIP sensor to EPN in the mixed solution containing 6×10^{-8} M EPN and 5-fold excess of IP, DA and NE. The MIP sensivity to EPN showed hardly any change in the presence of IP, DA and NE. It indicated a larger current toward EPN than other analogs, which proved the EPN molecularly imprinted sensor is highly specific to EPN.

Also, selectivity can be explained by calculating the imprinting factor (IF), which is described as the ratio of Δi_{MIP} to Δi_{NIP}. The IF for EPN is 8.14, but in the other interferences, it is 2.9, 1.73, 1.67, 1.4 and 1.1 for NE, DA, IP, AA, UA, respectively, which confirmed good selectively of the fabricated sensor for EPN (Fig. 10).

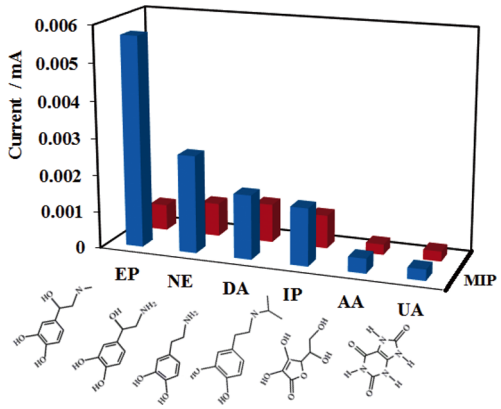

Fig. 10 Selectivity of the MIP and NIP sensor for EPN and interferences.

Under the optimized condition, sensitivity and linear range of MGR-AuNPs@NIP was studied using DPV. The linear range and slope of the calibration curve (sensitivity) were obtained as 4×10^{-8} – 3×10^{-7} M and 21.803, respectively. The linear range of the NIP sensor was lower than that of the MIP sensor, and the regression equation was ($I = 21.803C + 0.0004$ ($R^2 = 0.7994$)) (Fig. S4, Supporting Information). Reproducibility of the NIP sensor is poor, so the correlation coefficient was not suitable. Comparing the electrochemical signals of EPN in MGR-Ox-Au@MIP/CPE and MGROx-Au@NIP/CPE showed that the MIP sites are effective in increasing current and selectivity. The enhancement in peak current and shape of the curve confirms the role of MIP as recognition element in the fabrication of a selective sensor for determination of EPN.

An addition, incorporation of AuNPs into MIP was carried out to improve the electrochemical property of MIP. The CV signal at MGR-Au@MIP/CPE was higher than the signal at MGR@MIP/CPE. Therefore, integration of AuNPs could increase the electrochemical property of the nanocomposite, thus changing the performance of the sensor (Fig. S5, Supporting Information).

Sensor stability and repeatability

The repeatability of the fabricated sensor was examined by CV for five repeated measurements of 10^{-7} M of EPN with the same electrode. Also, five electrodes prepared independently under the same conditions were used to measure EPN. A relative standard deviation (RSD) of 2.14% for a peak current of EPN was obtained which indicates good repeatability of the modified sensor. The stability of this sensor was also studied; its signal response was approximately 95.6% of the initial value after storage for 60 days at room temperature, which demonstrates suitable stability of the sensor.

Measurement of EPN in real samples

In order to assess the applicability and reliability of the designed sensor, EPN was determined for blood serum and urine samples using standard addition under optimum conditions. The MIP has selectivity toward the EPN template molecule. Its specific identification is based on the interaction between template molecules and binding sites. The selectivity of this sensor is evaluated in the presence of species such as calcium, vitamin D, testosterone, progesterone, creatinine, cholesterol, and so on (Table 2). The response of this sensor toward the EPN molecule was much higher than the other species and had a good interaction between the binding sites and the EPN molecule, with the signal increasing with increasing EPN concentration. Its selectivity for the EPN is due to the shape of the cavities in the polymer, to which the molecule is well-fitted so that the other molecules can hardly be completed with polymer cavities. Accuracy and precision are calculated in Table 3. Good accuracy has been achieved in the measurement with recovery in the range of 96.4 to 101.05%. These results suggest that the proposed method can be used to analyze EPN in real samples.

Table 2 Results of molecular pathology laboratory tests on human blood serum and urine

Test	Result	Unit	Method
Calcium	8.8	mg/dL	Photometry
(25-OH) Vit D	45.0	ng/mL	Elisa
Cholesterol	175.0	mg/dL	CL[a]
Urea	36.0	mg/dL	Urease
17 OH progesteron	0.5	mg/mL	CL

a. Carbon labeled.

Table 3 Determination of EPN in real samples ($n = 3$)

Sample	Added/ 10^{-7} M	Found/ 10^{-7} M	Recovery, %	RSD, %
1 (urine)	0.9	0.829	98.1	1.42
2	2.5	2.43	97.3	2.77
3	3.5	3.37	96.4	2.27
1 (serum)	0.9	0.876	97.4	1.44
2	2.5	2.52	101.05	2.7
3	3.5	3.48	99.5	3.09

Conclusions

In this study, a new electrochemical sensor based on modified MGR-Ox-AuNP$_S$@MIP was designed to determine EPN in biological samples. To improve the conductivity of this electrochemical sensor, AuNP$_S$ were coated on the surface of GR-Ox due to the rapid transfer of electrons across the larger effective surface area. AuNP$_S$ and GR-Ox were used to increase the signal current of the electrochemical sensor, so its sensitivity has been improved. The research has shown the potential of this sensor to identify and determine EPN trace amounts in real samples. This sensor was easily constructed and showed good analytical efficiency.

Acknowledgements

Islamic Azad University, Tabriz Branch, Faculty of Science, Laboratory of Chemistry, supported this work.

Supporting Information

This material is available free of charge on the Web at http://www.jsac.or.jp/analsci/.

References

1. A. S. Al-Ayash, Y. H. Muhamad, and S. A. Gafori, *Baghdad Sci. J.*, **2011**, *8*, 110.
2. H. Montaseri, H. Khajehsharifi, and S. Yousefinejad, *Quím. Nova*, **2014**, *37*, 1404.
3. H. Jeong and S. Jeon, *Sensors*, **2008**, *8*, 6924.
4. P. S. Dorraji and F. Jalali, *Sens. Actuators, B*, **2014**, *200*, 251.
5. T. Thomas, R. J. Mascarenhas, O. J. D'Souza, S. Detriche, Z. Mekhalif, and P. Martis, *Talanta*, **2014**, *125*, 352.
6. A. S. Al-Ayash, *J. Al-Nahrain Univ.*, **2008**, *11*, 46.
7. J. B. Nevado, J. L. Gallego, and P. B. Laguna, *J. Pharm. Biomed. Anal.*, **1996**, *14*, 571.
8. J. Du, L. Shen and J. Lu, *Anal. Chim. Acta*, **2003**, *489*, 183.
9. A. M. Hansen, J. Kristiansen, J. L. Nielsen, K. Byrialsen, and J. M. Christensen, *Talanta*, **1999**, *50*, 367.
10. M. A. Fotopoulou and P. C. Ioannou, *Anal. Chim. Acta*, **2002**, *462*, 179.
11. H. Y. Wang, Y. Sun, and B. Tang, *Talanta*, **2002**, *57*, 899.
12. B. Li, Z. Zhang, and Y. Jin, *Biosens. Bioelectron.*, **2002**, *17*, 585.
13. D. W. Barnum, *Anal. Chim. Acta*, **1977**, *89*, 157.
14. M. Sorouraddin, J. Manzoori, E. Kargarzadeh, and A. H. Shabani, *J. Pharm. Biomed. Anal.*, **1998**, *18*, 877.
15. S. Wei, G. Song, and J. M. Lin, *J. Chromatogr. A*, **2005**, *1098*, 166.
16. F. Li, X. Jiang, J. Zhao, and S. Zhang, *Nano Energy*, **2015**, *16*, 488.
17. J. R. Potts, D. R. Dreyer, C. W. Bielawski, and R. S. Ruoff, *Polym. J.*, **2011**, *52*, 5.
18. J. Li, X. Zeng, T. Ren, and E. Van Der Heide, *Lubricants*, **2014**, *2*, 137.
19. J. Phiri, P. Gane, and T. C. Maloney, *Mater. Sci. Eng. B*, **2017**, *215*, 9.
20. Y. Li, X. Li, C. Dong, J. Qi, and X. Han, *Carbon*, **2010**, *48*, 3427.
21. Y. Shao, J. Wang, H. Wu, J. Liu, I. A. Aksay, and Y. Lin, *Electroanalysis*, **2010**, *22*, 1027.
22. B. Liu, H. Cang, and J. Jin, *Polymers*, **2016**, *8*, 309.
23. X. Su, X. Li, J. Li, M. Liu, F. Lei, X. Tan, P. Li, and W. Luo, *Food Chem.*, **2015**, *171*, 292.
24. Q. Zhou, Ch. Liu, H. Zhang, Ch. Zhao, and Y. Wang, *Anal. Sci.*, **2017**, *33*, 957.
25. L. Y. Mehmet, E. Tanju, and A. Necip, *Sens. Actuators, B*, **2015**, *210*, 149.
26. S. Dadkhah, E. Ziaei, A. Mehdinia, T. B. Kayyal, and A. Jabbari, *Microchim. Acta*, **2016**, *183*, 1933.
27. X. Li, X. Wang, L. Li, H. Duan, and C. Luo, *Talanta*, **2015**, *131*, 354.
28. X. Li and K. H. Row, *Anal. Sci.*, **2017**, *33*, 611.
29. T. Kubo, *Anal. Sci.*, **2017**, *33*, 1321.
30. R. Ahmad, N. b. w. Griffete, A. Lamouri, N. Felidj, M. M. Chehimi, and C. Mangeney, *Chem. Mater.*, **2015**, *27*, 5464.
31. H. Jiang, D. Jiang, J. Shao, and X. Sun, *Biosens. Bioelectron.*, **2016**, *75*, 411.
32. M. T. Jafari, B. Rezaei, and H. Bahrami, *Anal. Sci.*, **2018**, *34*, 297.
33. L. Shahriary and A. A. Athawale, *Int. J. Renew. Energy. Environ. Eng.*, **2014**, *2*, 58.
34. J. F. V. Pilsum, R. Martin, E. Kito, and J. Hess, *J. Biol. Chem.*, **1956**, *222*, 225.
35. T. M. Alshammari, A. A. Al-Hassan, T. B. Hadda, and M. Aljofan, *Saudi Pharm. J.*, **2015**, *23*, 689.
36. T. F. Yeh, C. Jaroslav, C. Chih-Yung, C. Ching, and T. Hsisheng, *Mater. Today*, **2013**, *16*, 78.
37. K. Saha, S. S. Agasti, C. Kim, X. Li, and V. M. Rotello, *Chem. Rev.*, **2012**, *112*, 2739.
38. M. Rahimnejad, S. K. Hassaninejad-Darzi, P. Izadi, and A. Asghar, *Anal. Bioanal. B*, **2015**, *7*, 370.
39. L. Jothi, N. Jayakumar, S. Jaganathan, and G. Nageswaran, *Mater. Res. Bull.*, **2018**, *98*, 300.
40. N. B. Messaoud, M. E. Ghica, C. Dridi, M. B. Ali, and C. M. Brett, *Sens. Actuators, B*, **2017**, *253*, 513.
41. Y. Hu, F. Li, X. Bai, D. Li, S. Hua, K. Wang, and L. Niu, *Chem. Commun.*, **2011**, *47*, 1743.
42. A. Afkhami, H. Ghaedi, T. Madrakian, M. Ahmadi, and H. Mahmood-Kashani, *Biosens. Bioelectron.*, **2013**, *44*, 34.
43. N. Ermiş and N. Tınkılıç, *Int. J. Electrochem. Sci.*, **2018**, *13*, 2286.
44. L. Wang, J. Bai, P. Huang, H. Wang, L. Zhang, and Y. Zhao, *Int. J. Electrochem. Sci.*, **2006**, *1*, 238.
45. M. Mazloum-Ardakani, A. Sadeghiane, S. Moosavizadeh, M. A. Karimi, and H. Mashhadizadeh, *Anal. Bioanal. Electrochem.*, **2009**, *1*, 224.
46. R. Cisternas, H. Kahlert, H. Wulff, and F. Scholz, *Electrochem. Commun.*, **2015**, *56*, 37.
47. E. Laviron, *J. Electroanal. Chem.*, **1979**, *101*, 19.
48. E. Chrzescijanska, E. Wudarska, E. Kusmierek, and J. Rynkowski, *J. Electroanal. Chem.*, **2014**, *713*, 17.
49. T. M. Narayana, P. Reddy, M. Gopal, M. Reddy, and G. R. Naidu, *Mater. Sci. Eng. C*, **2015**, *56*, 57.
50. A. Gorczyński, M. Kubicki, K. Szymkowiak, T. Łuczak, and V. Patroniak, *RSC Adv.*, **2016**, *6*, 101888.
51. Z. Li, K. Ma, Zh. Cheng, C. Yan, and G. Liu, *Int. J. Electrochem. Sci.*, **2017**, *12*, 2389.
52. X. Li, M. Chen, X. Ma, and X. Lin, *Int. J. Chem.*, **2010**, *2*, 206.
53. M. Mazloum-Ardakani, H. Beitollahi, M. K. Amini, B. F. Mirjalili, and F. Mirkhalaf, *J. Electroanal. Chem.*, **2011**, *651*, 243.
54. H. Vieira and O. Fatibello-Filho, *Ecletica Quim.*, **2004**, *29*, 79.